

Gas–liquid phase equilibrium in ionic fluids: Coulomb versus non-Coulomb interactions

O. Patsahan

Institute for Condensed Matter Physics of the National Academy of Sciences of Ukraine,
1 Svientsitskii St., 79011 Lviv, Ukraine

Received August 28, 2014, in final form November 10, 2014

Using the collective variables theory, we study the effect of competition between Coulomb and dispersion forces on the gas–liquid phase behaviour of a model ionic fluid, i.e. a charge-asymmetric primitive model with additional short-range attractive interactions. Both the critical parameters and the coexistence envelope are calculated in a one-loop approximation as a function of the parameter α measuring the relative strength of the Coulomb to short-range interactions. We found the very narrow region of α bounded from the both sides by tricritical points which separates the models with “nonionic” and “Coulombic” phase behaviour. This is at variance with the result of available computer simulations where no tricritical point is found for the finely-discretized lattice version of the model.

Key words: ionic fluids, gas–liquid phase diagram, tricritical point, Coulomb interactions, short-range attraction

PACS: 05.70.Fh, 64.60.De, 64.60.Kw

1. Introduction

Critical and phase behaviour of ionic fluids has been intensively studied for the last decades. These studies were stimulated by earlier experiments on ionic solutions that yielded three types of critical behavior: mean-field and Ising-like behavior as well as crossover between the two [1, 2]. In accordance with these peculiarities, ionic solutions were conventionally divided into two classes, namely: “solvophobic” systems with Ising-like critical behavior in which Coulomb forces are not supposed to play a major role (the solvent is generally characterized by high dielectric constant) and “Coulombic” systems in which the phase separation is primarily driven by Coulomb interactions (the solvent is characterized by low dielectric constant) [2, 3]. The critical behaviour of the Coulombic systems has been a subject of great debates. At present, the analysis of the existing experimental data for Coulombic and solvophobic systems has shown that the asymptotic critical behaviour is Ising-like for both classes [4, 5]. Experiments that supported the expectation of mean-field critical behaviour could not be reproduced in later works [6–8]. Strong evidence for the Ising universal class for the Coulombic fluids has been also found by recent simulations [9–12] and theoretical studies [13–15]. More recent accurate experiments indicate in general a crossover to the mean-field behaviour, where the non-classical region increases with the polarity of the solvent [5, 16, 17]. Theoretical predictions of such behaviour has been recently given in [18, 19].

In this paper we continue our systematic study of the phase behaviour of ionic fluids. Our aim is to study the effect of the strength of electrostatic interactions (the dielectric constant of the solvent) on the phase separation in ionic solutions. It should be noted that ionic and nonionic (“classical”) fluids differ greatly in the strength of the interactions. In simple neutral fluids, the interaction energy is of the order of the thermal energy, i.e., the reduced temperature $T^* = k_B T / \phi_{\min} \approx 1$ (ϕ_{\min} is the depth of the interaction potential at its minimum). By contrast, in typical molten salts, the interionic interactions are more than one order of magnitude larger than $k_B T$, i.e., $T^* \ll 1$. In electrolyte solutions, the strength of the Coulomb interactions depends on the dielectric constant of the solvent. In addition, the phase diagrams of Coulomb dominated fluids are quite asymmetric when compared to nonionic fluids [20–22].

The evolution of the gas–liquid phase diagram of the charged Yukawa fluid with an increase of ionic interactions was studied in [23] using both the mean-spherical approximation and the Gibbs ensemble Monte Carlo simulations. It has been found that the gas–liquid coexistence envelope changes from a “nonionic type” (such as that of the one-component Yukawa fluid) to a “Coulombic type” (such as that of the primitive model) when the strength of the Coulomb interactions is increased. However, the issue of the watershed between the nonionic and ionic phase behaviour (the “solvophobic” and “Coulombic” systems) has not been addressed so far. Here, we address this issue using a simple model of ionic fluids, i.e., the charge-asymmetric primitive model (PM) supplemented by short-range attractive interactions where the short-range attraction is considered as an approximation to van der Waals interactions [18, 23–27]. The model without the Coulomb interactions (a hard-sphere square-well model) exhibits a gas–liquid coexistence typical of nonionic (“solvophobic”) fluids. Another limiting model, i.e., the PM, demonstrates the “Coulombic” phase diagram. A theoretical background for this study is the statistical field theory that exploits the method of collective variables (CVs) [29–32]. The theory enables us to derive an exact expression for the functional of grand partition function of the model and on this basis to develop the perturbation theory [32, 33]. The well-known approximations for the free energy, in particular Debye–Hückel limiting law and the mean spherical approximation, can be reproduced within the framework of this theory [33]. Links between this approach and the field theoretical approach [34] were established in [35] for the case of the RPM. Using the CVs theory we have recently derived a microscopic-based effective Hamiltonian for the model with short- and long-range interactions [18]. A distinguishing feature of the developed approach is that it enables one to obtain the coefficients of the Hamiltonian, including the square-gradient term, within the framework of the same approximation. For the above-mentioned model, we have found explicit expressions for all the relevant coefficients in the one-loop approximation [18]. For the free energy, this approximation coincides with the well-known random-phase approximation (RPA) and, thus, produces the mean-field phase diagram. Here, we use the effective Hamiltonian derived in [18] to study the gas–liquid phase behaviour of the model with parameters ranging from the purely non-Coulombic regime to the purely Coulombic regime.

The paper is arranged as follows. A theoretical background is given in section 2. The results for the gas–liquid critical parameters and phase diagrams are presented in section 3. Concluding remarks are made in section 4.

2. Theory

2.1. Model

We start with a two-component model of ionic fluids. The pair interaction potential is assumed to be of the following form:

$$U_{\alpha\beta}(r) = \phi_{\alpha\beta}^{\text{HS}}(r) + \phi_{\alpha\beta}^{\text{SR}}(r) + \phi_{\alpha\beta}^{\text{C}}(r), \quad (2.1)$$

where $\phi_{\alpha\beta}^{\text{HS}}(r)$ is the interaction potential between the two additive hard spheres of diameters σ_α and σ_β . The potential $\phi_{\alpha\beta}^{\text{SR}}(r)$ describes the short-range (van der Waals-like) attraction. $\phi_{\alpha\beta}^{\text{C}}(r)$ is the Coulomb potential: $\phi_{\alpha\beta}^{\text{C}}(r) = q_\alpha q_\beta \phi^{\text{C}}(r)$, where $\phi^{\text{C}}(r) = 1/(\epsilon r)$ and ϵ is the dielectric constant of the solvent. The ions of the species $\alpha = 1$ carry an electrostatic charge $q_+ = q_0$ and those of species $\alpha = 2$ carry an opposite charge $q_- = -z q_0$ (q_0 is an elementary charge and z is the parameter of charge asymmetry). Overall charge neutrality requires that $q_+ N_+ + q_- N_- = 0$, where N_+ and N_- are, respectively, the number of positive and negative ions. In general, the binary system of hard spheres interacting via the potential $\phi_{\alpha\beta}^{\text{SR}}(r)$ can exhibit both the gas–liquid and demixion phase transitions. Thus, we simplify the model assuming that (i) the hard spheres are of the same diameter $\sigma_\alpha = \sigma_\beta = \sigma$ and (ii) $\phi_{11}^{\text{SR}}(r) = \phi_{22}^{\text{SR}}(r) = \phi_{12}^{\text{SR}}(r) = \phi^{\text{SR}}(r)$. With these restrictions, the uncharged system can only exhibit a gas–liquid phase separation and a possible demixion is ruled out. Then, we specify $\phi^{\text{SR}}(r)$ in the form of the square-well (SW) potential of depth ϵ and range λ . The system of hard spheres interacting through the SW potential with $\lambda = 1.5\sigma$ can serve as a reasonable model for simple (nonionic) fluids.

It is worth noting that in the treatments of models with hard cores, the perturbation potential is not defined uniquely inside the hard core. Here, we use the Weeks-Chandler-Andersen regularization scheme

for the both potentials $\phi^C(r)$ and $\phi^{SR}(r)$ [36]. In this case, the Fourier transforms of these potentials have the form:

$$\tilde{\phi}^{SR}(k) = -\epsilon\sigma^3 \frac{4\pi}{x^3} [-\lambda x \cos(\lambda x) + \sin(\lambda x)] \quad (2.2)$$

and

$$\tilde{\phi}^C(k) = 4\pi\sigma^3 \frac{\sin(x)}{\epsilon x^3}, \quad (2.3)$$

where $x = k\sigma$.

2.2. Effective Hamiltonian near the gas-liquid critical point

We consider the model (2.1)–(2.3) near the gas-liquid critical point. Using the method of collective variables, we can present the effective Ginzburg-Landau Hamiltonian of the model as follows (see [18] and references therein):

$$\begin{aligned} \mathcal{H}^{\text{eff}} = & a_{1,0}\rho_{0,N} + \frac{1}{2!\langle N \rangle} \sum_{\mathbf{k}} (a_{2,0} + k^2 a_{2,2}) \rho_{\mathbf{k},N} \rho_{-\mathbf{k},N} + \frac{1}{3!\langle N \rangle^2} \sum_{\mathbf{k}_1, \mathbf{k}_2} a_{3,0} \\ & \times \rho_{\mathbf{k}_1, N} \rho_{\mathbf{k}_2, N} \rho_{-\mathbf{k}_1 - \mathbf{k}_2, N} + \frac{1}{4!\langle N \rangle^3} \sum_{\mathbf{k}_1, \mathbf{k}_2, \mathbf{k}_3} a_{4,0} \rho_{\mathbf{k}_1, N} \rho_{\mathbf{k}_2, N} \rho_{\mathbf{k}_3, N} \rho_{-\mathbf{k}_1 - \mathbf{k}_2 - \mathbf{k}_3, N} + \dots, \end{aligned} \quad (2.4)$$

where $\rho_{\mathbf{k},N}$ is the collective variable (CV) which describes the value of the \mathbf{k} -th fluctuation mode of the total number density. In a one-loop approximation, the coefficients of Hamiltonian (2.4) have the form:

$$a_{1,0} = -\Delta v_N + \beta\rho\tilde{\phi}^{SR}(0) - \tilde{C}_{1,C}, \quad (2.5)$$

$$a_{2,0} = -\rho\tilde{C}_{2,HS} + \beta\rho\tilde{\phi}^{SR}(0) - \rho\tilde{C}_{2,C}, \quad (2.6)$$

$$a_{2,2} = -\frac{1}{2}\rho\tilde{C}_{2,HS}^{(2)} + \frac{1}{2}\beta\rho\tilde{\phi}^{SR,(2)} - \frac{1}{4\langle N \rangle} \sum_{\mathbf{q}} \tilde{g}^{(2)}(\mathbf{q}) [1 + \tilde{g}(\mathbf{q})], \quad (2.7)$$

$$a_{n,0} = -\rho^{n-1}\tilde{C}_{n,HS} - \rho^{n-1}\tilde{C}_{n,C}, \quad n \geq 3. \quad (2.8)$$

Here, we introduce the following notations. The subscript HS refers to the hard-sphere system and the superscript (2) in equation (2.7) denotes the second-order derivative with the respect of the wave vector k : $\tilde{g}^{(2)}(\mathbf{q}) = \partial^2 \tilde{g}(|\mathbf{q} + \mathbf{k}|) / \partial k^2|_{k=0}$, $\tilde{C}_{2,HS}^{(2)} = \partial^2 \tilde{C}_{2,HS}(k) / \partial k^2|_{k=0}$, and $\tilde{\phi}^{SR,(2)} = \partial^2 \tilde{\phi}^{SR}(k) / \partial k^2|_{k=0}$.

The addend Δv_N in equation (2.5) is related to the chemical potentials

$$\Delta v_N = v_N - v_{N,HS}, \quad v_N = \frac{z\tilde{v}_1 + \tilde{v}_2}{1+z}, \quad (2.9)$$

where \tilde{v}_α is determined by

$$\tilde{v}_\alpha = v_\alpha + \frac{\beta}{2V} \sum_{\mathbf{q}} [\tilde{\phi}^{SR}(\mathbf{q}) + q_\alpha^2 \tilde{\phi}^C(\mathbf{q})], \quad (2.10)$$

v_α is the dimensionless chemical potential, $v_\alpha = \beta\mu_\alpha - 3\ln\Lambda_\alpha$ and μ_α is the chemical potential of the α th species; $\beta = 1/k_B T$ is the reciprocal temperature; $\Lambda_\alpha^{-1} = (2\pi m_\alpha \beta^{-1} / h^2)^{1/2}$ is the inverse de Broglie thermal wavelength.

$\tilde{C}_{n,HS}$ is the Fourier transform of the n -particle direct correlation function of a one-component hard-sphere system at $k = 0$, $\rho = \langle N \rangle / V = \rho_1 + \rho_2$ is the total number density. Explicit expressions for $\tilde{C}_{n,HS}$ and $\tilde{C}_{2,HS}^{(2)}$ for $n \leq 4$ in the Percus-Yevick (PY) approximation are given in reference [18] (see appendix in [18]).

The last term on the right-hand side of equations (2.5)–(2.8) results from the charge-charge correlations being taken into account through integration over the charge subsystem [18]. In particular, $\rho^{n-1}\tilde{C}_{n,C}$ reads

$$\rho^{n-1}\tilde{C}_{n,C} = \frac{(n-1)!}{2} \frac{1}{\langle N \rangle} \sum_{\mathbf{q}} [\tilde{g}(\mathbf{q})]^n, \quad (2.11)$$

where

$$\tilde{g}(q) = -\frac{\beta\rho\tilde{\phi}^C(q)}{1 + \beta\rho\tilde{\phi}^C(q)}. \quad (2.12)$$

All the coefficients in equation (2.4) except $a_{2,2}$ describing the square-gradient term can be obtained from the one-loop (RPA) free energy [18]

$$a_{n,0} = \rho^{n-1} \frac{\partial^n (-\beta f_{\text{RPA}})}{\partial \rho^n} = \rho^{n-1} \tilde{C}_n(0, \dots), \quad n \geq 2,$$

where $\tilde{C}_n(0, \dots)$ denotes the Fourier transform of the n -particle direct correlation function of the full system in the long-wavelength limit. It is worth noting that the functions \tilde{C}_n differ from the ordinary direct correlation functions \tilde{c}_n by an ideal term [37]. Equation $a_{2,0} = 0$ yields a spinodal curve. In combination with equation $a_{3,0} = 0$ it determines the critical point.

The square-gradient term $a_{2,2}$ given by equation (2.7) is also derived in the one-loop approximation (see [18] for details). It is essential that the last addend on the right-hand side of (2.7) describes the short range attraction which arises from the integration over the charge subsystem. We emphasize that although the original Hamiltonian of the purely Coulombic model [$\phi_{\alpha\beta}^{\text{SR}}(r) = 0$] does not include direct pair attractive interactions of number density fluctuations, the effective short-range attraction does appear in the effective Hamiltonian (2.4). It is worth noting that the expression for $a_{2,2}$ given by (2.7) produces a correct result for the density correlation length ξ in the limit of charged point particles (see [18] and references herein).

Coefficient $a_{1,0}$ is the excess part of the chemical potential v_N connected with the short-range attractive and long-range Coulomb interactions. Equation $a_{1,0} = 0$ yields the expression for the chemical potential in the RPA.

It is worth noting that there is no difference between the charge-asymmetric PM and the restricted primitive model (RPM) having $z = 1$ at this level of approximation [33, 38–40]. Hereafter, we briefly refer to the model (2.1)–(2.3) as a RPM-SW model.

3. Gas-liquid phase diagram

Here, we study the gas-liquid phase diagram of the the RPM-SW model for the model parameters ranging from the RPM limit to the SW limit. Using equations (2.2)–(2.3) and (2.9)–(2.12) we rewrite the expressions for the coefficients of the effective Hamiltonian [see (2.5)–(2.8)] as follows:

$$a_{1,0} = -v_N + v_{N,\text{HS}} + \frac{1}{2\alpha T^C} - \frac{1}{2T^C} - \frac{8\eta\lambda^3}{\alpha T^C} + i_1, \quad (3.1)$$

$$a_{2,0} = -\rho \tilde{C}_{2,\text{HS}} - \frac{8\eta\lambda^3}{\alpha T^C} + i_2, \quad (3.2)$$

$$a_{2,2} = -\frac{1}{2}\rho \tilde{C}_{2,\text{HS}}^{(2)} + \frac{4}{5} \frac{\eta\lambda^5}{\alpha T^C} - \frac{1}{6\pi T^C} i_{12}, \quad (3.3)$$

$$a_{n,0} = -\rho^{n-1} \tilde{C}_{n,\text{HS}} + i_n, \quad n \geq 3, \quad (3.4)$$

where [18]

$$i_n = \frac{(n-1)!(-\kappa^2)^{n-1}}{\pi T^C} \int_0^\infty x^2 \left[\frac{\sin(x)}{x^3 + \kappa^2 \sin(x)} \right]^n dx, \quad (3.5)$$

$$i_{12} = \int_0^\infty x^6 \left\{ \kappa^2 x^2 [1 + \cos^2(x)] + 2[x^3 - 2\kappa^2 \sin(x)] [2x \cos(x) - 3 \sin(x)] + x^5 \sin(x) \right\} / [x^3 + \kappa^2 \sin(x)]^4 dx, \quad (3.6)$$

and $\kappa = \kappa_D \sigma$ with κ_D being the Debye number. In equations (3.1)–(3.6), T^C is the reduced temperature defined as the ratio between the thermal energy $k_B T$ and the Coulomb energy of the opposite charged hard spheres at contact, $E^C = zq_0^2/\epsilon\sigma$,

$$T^C = \frac{k_B T}{E^C} = \frac{k_B T \epsilon \sigma}{z q_0^2}, \quad (3.7)$$

α is the ratio of the Coulomb and square-well energies at contact

$$\alpha = \frac{E^C}{\epsilon} = \frac{z q_0^2}{\epsilon \sigma \epsilon}, \quad (3.8)$$

and $\eta = \pi \rho \sigma^3/6$ is the packing fraction of the ions. For ϵ being fixed, α measures the strength of the Coulomb interactions. In this case, either the increase of ion charges or the decrease of dielectric constant for fixed charges results in the increase of the parameter α . It is worth noting that $a_{n,0}$ with $n \geq 3$ is independent of α when the reduced temperature is given by equation (3.7). The approximation (3.1)–(3.6) produces the mean-field phase diagram.

First, we consider the critical point. At the critical point, the system of equations

$$a_{2,0}(\rho_c, T_c) = 0, \quad a_{3,0}(\rho_c, T_c) = 0 \quad (3.9)$$

holds yielding the critical temperature and the critical density for the fixed α . Generally, the curve given by the second equation of (3.9) intersects the spinodal twice, i.e., at its maximum and minimum points (see figure 1). The gas-liquid critical point is located at the maximum point of the spinodal. The results for the gas-liquid critical parameters are displayed in figures 2–4.

In figure 2, the dependence of the reduced critical temperature given by (3.7) on the parameter $\alpha^{-1} \sim \epsilon$ is shown. As is seen, T_c^C increases almost linearly with an increase of the dielectric constant. The trend of T_c^C agrees with the experimental observations when one expresses the critical temperature of real ionic solutions in the RPM values [16, 41]. When the strength of the Coulomb interactions increases, ($\alpha^{-1} \rightarrow 0$) T_c^C converges to the RPM limit $T_c^C = 0.08446$ [18].

In order to compare our results with the available results of computer simulations [27] we rewrite the reduced temperature in equation (3.7) as $k_B T/\epsilon$, the usual definition for the SW potential. Figure 3 shows that the critical temperature scaled by the SW depth ϵ rapidly decreases with a decrease of the Coulomb interactions and then slowly approaches the SW limit $k_B T_c/\epsilon = 1.2667$ [18]. Such behaviour is in agreement with the results of simulations [27].

The dependence of the reduced critical density $\rho_c^* = \rho_c \sigma^3$ on the parameter α^{-1} is shown in figure 4. For very small α^{-1} , ρ_c^* increases slowly from the RPM value $\rho_c^* \simeq 0.009$ and then at $\alpha^{-1} \simeq 0.048$ changes sharply to the value about 20 times larger than the RPM limit. For $\alpha^{-1} > 0.048$, the critical density approaches the SW limit $\rho_c^* = 0.2457$ passing through a shallow minimum located at $\alpha^{-1} \simeq 0.1$. Just

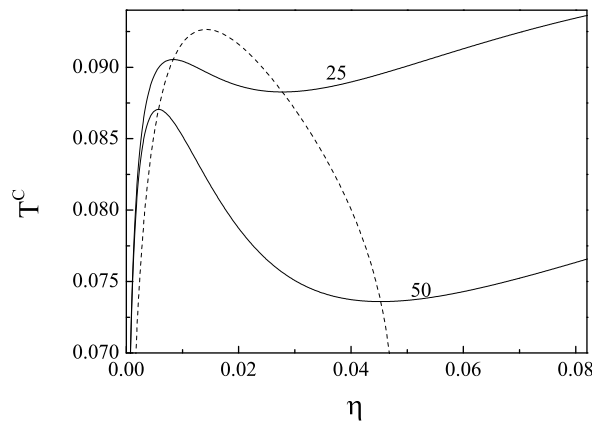


Figure 1. RPM-SW model: the loci of equations $a_{2,0} = 0$ (solid lines) and $a_{3,0} = 0$ (dashed line) for $\alpha = 25$ and 50. T^C is given by equation (3.7), $\eta = \pi \rho \sigma^3/6$ is the packing fraction and $\alpha = q_0^2 z / (\epsilon \sigma \epsilon)$.

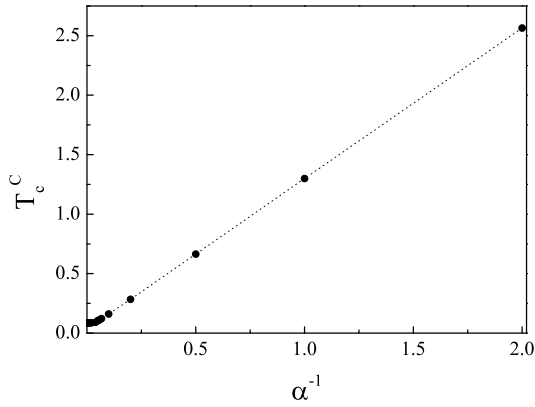


Figure 2. Reduced critical temperature T_c^C of the RPM-SW model as a function of $\alpha^{-1} \sim \epsilon$ [see equation (3.8)]. The line is a guide to the eye.

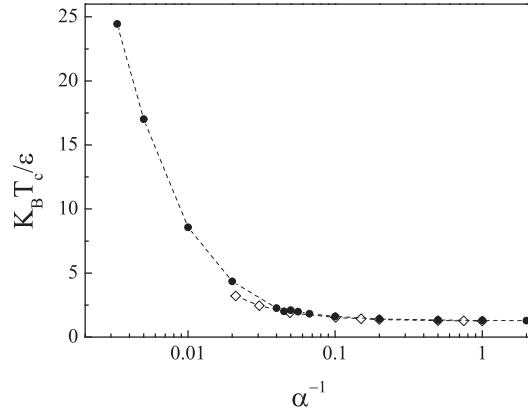


Figure 3. Reduced critical temperature $k_B T_c / \epsilon$ of the RPM-SW model as a function of $\alpha^{-1} \sim \epsilon$ [see equation (3.8)]. Full circles are the results of the present work; open diamonds correspond to the results of simulations [27]. The line is a guide to the eye.

as standard mean-field theories, the one-loop approximation considered in this paper underestimates the critical number density, the deviation from the simulation data increases when the strength of the Coulomb interactions becomes sufficiently large [23, 40, 42]. At the same time, our results demonstrate the behaviour of ρ_c^* for small α^{-1} which qualitatively differs from the available results of computer simulations (see [27]). In simulations, the critical density rather rapidly increases with α^{-1} in the region $\alpha^{-1} \leq 0.1$ but it does not exhibit a jump. It is worth noting that the behaviour of ρ_c^* for $\alpha^{-1} > 0.1$ qualitatively agrees with the results of simulations.

It is instructive to view the range of the effective density-density interactions $R_N = \sqrt{a_{2,2}/\sigma}$ [see equation (3.3)] as a function of α^{-1} . Figure 5 shows the behaviour of $R_{N,c} = R_N(T_c, \rho_c)$ with the variation of α^{-1} . The dimensionless amplitude of the density correlation length

$$\xi_0^* = \frac{\xi_0}{\sigma} = \frac{1}{\sigma} \sqrt{\frac{a_{2,2}}{a_{2,t}}}, \quad a_{2,t} = \left. \frac{\partial a_{2,0}}{\partial t} \right|_{t=0}$$

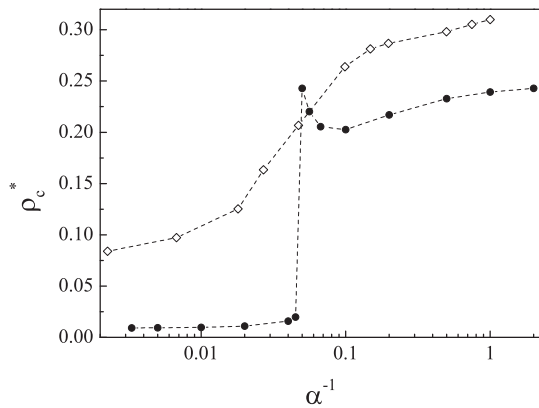


Figure 4. Reduced critical density $\rho_c^* = \rho_c \sigma^3$ of the RPM-SW model as a function of $\alpha^{-1} \sim \epsilon$ [see equation (3.8)]. Full circles are the results of the present work; open diamonds correspond to the results of simulations [27]. The line is a guide to the eye.

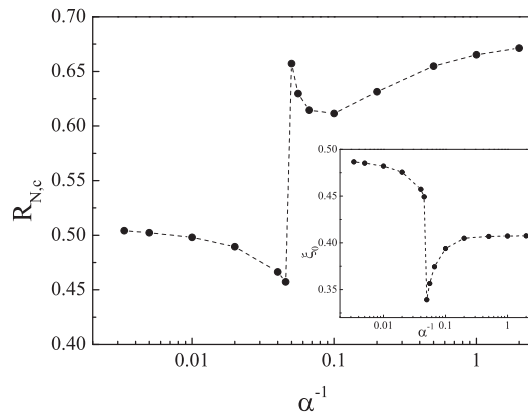


Figure 5. Dimensionless range of the effective density-density interaction $R_{N,c} = R_N(T_c, \rho_c)$ of the RPM-SW model as a function of $\alpha^{-1} \sim \epsilon$ [see equation (3.8)]. The inset shows the dimensionless amplitude of the correlation length ξ_0^* as a function of α^{-1} . The line is a guide to the eye.

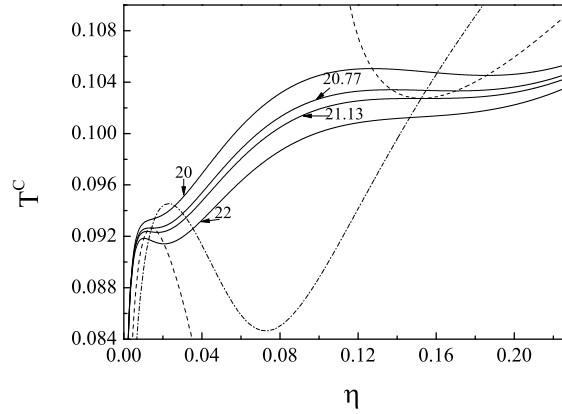


Figure 6. RPM-SW models with $\alpha = 20$, $\alpha = 20.77$, $\alpha = 21.13$, and $\alpha = 22$: the loci of equations $a_{2,0} = 0$ (solid lines), $a_{3,0} = 0$ (dashed lines) and $a_{4,0} = 0$ (dash-dotted line). T^C is given by equation (3.7), $\eta = \pi\rho\sigma^3/6$ is the packing fraction and $\alpha = q_0^2 z / (\epsilon\sigma\epsilon)$.

as a function of α^{-1} is shown in the inset. Remarkably, the trends of $R_{N,c}$ and ρ_c^* are very similar, especially for $\alpha^{-1} > 0.048$. Furthermore, the behaviour of $R_{N,c}$ clearly shows the two distinctive regions separated by $\alpha^{-1} \simeq 0.048$: the region where $R_{N,c} \lesssim 0.5$ and the region where $R_{N,c} > 0.6$. Similarly, the two distinctive branches are clearly seen in the behaviour of ξ_0^* . This implies that $\alpha^{-1} \simeq 0.048$ ($\alpha \simeq 21$) separates the models which demonstrate non-Coulombic phase behaviour (“solvophobic systems”) from the models demonstrating Coulombic phase behaviour (“Coulombic systems”).

Let us scrupulously consider the RPM-SW models with α close to $\alpha = \alpha^* \simeq 21$ ($(\alpha^*)^{-1} \simeq 0.048$). To this end, we solve the equation

$$a_{4,0}(\rho_c, T_c) = 0 \quad (3.10)$$

additionally to the system of equations (3.9). The results are shown in figure 6. The solid curves in the figure are the spinodals of the RPM-SW models with $\alpha = 20, 20.77, 21.13$, and 22 . The two dashed curves, a curve with a maximum in the region of low temperatures and low densities and another curve with a minimum in the region of higher temperatures and moderate densities, indicate the loci of equation $a_{3,0} = 0$. The spinodal of the RPM-SW model with $\alpha = 22$ intersects the low-density dashed curve while the spinodal corresponding to $\alpha = 20$ intersects the moderate-density dashed curve. For $\alpha = 21.13$, the spinodal intersects the low-density curve and it is tangent to the curve placed at higher densities. The opposite situation appears for $\alpha = 20.77$: the spinodal is tangent to the low-density dashed curve and intersects another dashed curve located at higher densities. The dash-dotted curve which presents the loci of equation (3.10) crosses the dashed curves at their extremum points (exactly at the points of tangency of the solid and dashed curves). These special points, at which equations (3.9) and equation (3.10) hold are called tricritical points [43]. The coordinates of the tricritical points are presented in table 1. The two tricritical points can be considered as limiting points which separate the low-density family of gas-liquid phase diagrams from the gas-liquid phase diagrams located at moderate densities. It should be noted that both a critical point and a tricritical point were predicted theoretically [24–26] and found in computer simulations [27] for the lattice RPM supplemented by short-range interactions. In these works, the tricritical point is associated with the transition to the charge-ordered phase. Besides, the tricritical point

Table 1. The reduced parameters of the tricritical points for the RPM-SW model. The reduced critical temperature T^C is given by (3.7) and $T^{\text{SR}} = k_B T / \epsilon$.

α	T_{trc}^C	$T_{\text{trc}}^{\text{SR}}$	ρ_{trc}^*
20.77	0.0926	1.9233	0.0269
21.13	0.1027	2.1701	0.2905

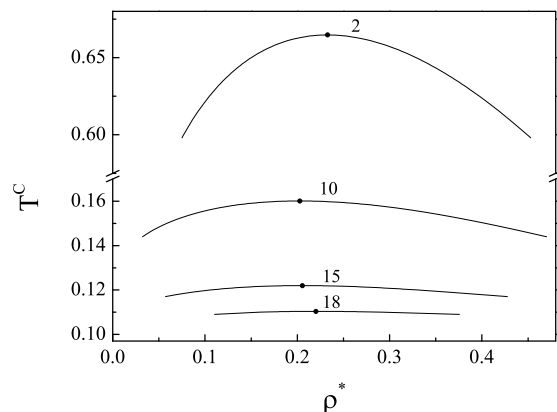


Figure 7. Gas-liquid coexistence curves of the RPM-SW model for $\alpha = 2, 10$ and 15 in the (T^C, ρ^*) representation. Full circles denote the location of the critical point.

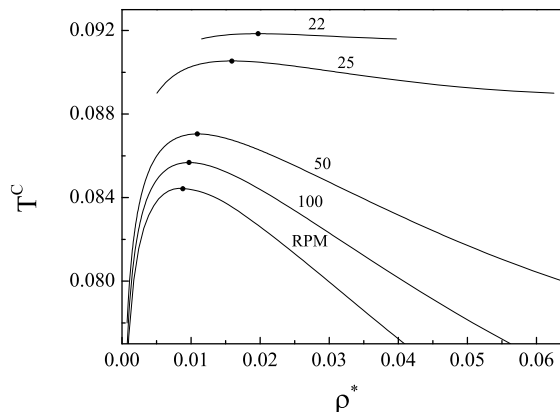


Figure 8. Gas-liquid coexistence curves of the RPM-SW model for $\alpha = 22, 25, 50$ and 100 in the (T^C, ρ^*) representation. Full circles denote the location of the critical point.

studied in [24–26] is either stable or metastable. On the other hand, no tricritical point was found in [27] for the lattice version of the RPM-SW model with the lattice discretization parameter $\zeta = 10$. According to [28], for $\zeta \geq 3$ the phase behaviour of the lattice RPM is qualitatively identical to the continuous model. Here, we focus our attention only on the gas-liquid equilibrium. The description of a possible existence of other phases requires going beyond the treatment presented in this work.

Now we study the evolution of the gas-liquid coexistence curves with the variation of α . To this end, we use equation (3.1) for the calculation of the chemical potential and employ the Maxwell double-tangent construction. Figures 7 and 8 show the coexistence curves of the RPM-SW models in the (T^C, ρ^*) plane for two sets of α corresponding to $\alpha < \alpha^*$ and $\alpha > \alpha^*$, respectively. Figure 7 shows almost symmetrical coexistence envelopes typical of non-Coulombic systems. In figure 8, the coexistence curves become more and more asymmetric with an increase of α and resemble the RPM coexistence curve at $\alpha > 100$. On the other hand, the coexistence region of the RPM-SW model reduces when α tends to α^* (from the both sides) indicating the approach of the tricritical point.

Therefore, our results suggest that the RPM-SW models with $\alpha \leq 20.77$ belong to the non-Coulombic systems in which the phase separation is driven by short-range forces while the RPM-SW models with $\alpha \geq 21.13$ belong to the Coulomb dominated systems. The two families of models are separated by a very narrow region of α bounded by the tricritical points.

4. Conclusions

We have studied the effect of the strength of the Coulomb interaction on the gas-liquid phase diagram of a model fluid. The model, referred to as RPM-SW model, consists of oppositely charged hard spheres of the same diameter with additional short-range attractive interactions. The short-range attraction is chosen in the form of the SW potential of the range $\lambda = 1.5\sigma$. Having introduced the parameter α that determines the strength of the Coulomb interaction with respect to the short-range SW interaction, we calculate the gas-liquid phase diagrams for α varying from 0 (the purely nonionic system) to ∞ (the purely Coulombic system). It is worth noting that the parameter α is proportional to the inverse dielectric constant of the solvent ϵ when the ion charges are fixed.

Both the coexistence envelopes and the critical parameters have been calculated in a one-loop approximation which is equivalent to the random phase approximation. We have found that the very narrow region of α ($20.77 \leq \alpha \leq 21.13$) separates the models demonstrating a nonionic type of phase behaviour from the models which demonstrate a ‘‘Coulombic’’ type of phase diagrams. This region is bounded from the both sides by the tricritical points: one point located at $T_{\text{trc},1}^{\text{SR}} = 1.9233$ and $\rho_{\text{trc},1}^* = 0.0269$ and another

point with the coordinates $T_{\text{trc},2}^{\text{SR}} = 2.1701$ and $\rho_{\text{trc},2}^* = 0.2905$. The dependence of the reduced critical temperature on α (α^{-1}) indicates a continuous variation from a phase transition driven by Coulomb interactions to a transition determined by “solvophobic” interactions. Such behaviour agrees with the available data of computer simulations performed for the lattice version of the RPM-SW model with high values of the lattice discretization parameter ζ ($\zeta = \sigma/l = 10$) [27]. On the other hand, the reduced critical density ρ_c^* sharply changes with α in the region between the two tricritical points. This is at variance with the results of computer simulations mentioned above. Furthermore, no tricritical points were found for the lattice version of the model in the high ζ case in the computer simulations

We have studied the range of the effective density-density interaction $R_{N,c}$ with the variation of α (α^{-1}). The results clearly indicate the two distinctive regions in the phase diagram ($R_{N,c} \lesssim 0.5$ and $R_{N,c} \gtrsim 0.6$) which are separated by $\alpha \approx 21$. The amplitude of the density correlation length ξ_0^* also shows different trends for $\alpha < 21$ and $\alpha > 21$. It should be noted that the values of ξ_0^* are larger for the Coulomb-dominated systems than for the non-Coulombic systems. The opposite situation takes place for $R_{N,c}$.

Thus, we have obtained the results for a phase behaviour of the RPM-SW model that qualitatively differ from the findings of the available computer simulations. Further investigations are needed in order to confirm (or rule out) the presence of the tricritical points in the model with $\alpha \approx 21$. In particular, higher-order approximations for the coefficients of the effective Hamiltonian (2.4) should be considered. On the other hand, it would be useful to perform computer simulations for the model parameters for which the theory predicts tricritical points.

References

1. Singh R.R., Pitzer K.S., J. Chem. Phys., 1990, **92**, 6775; doi:10.1063/1.458263.
2. Levelt Sengers J.M.H., Given J.A., Mol. Phys., 1993, **80**, 899; doi:10.1080/00268979300102751.
3. Weingärtner H., Merkel T., Maurer U., Conzen J.-P., Glasbrenner H., Käshammer S., Ber. Bunsenges. Phys. Chem., 1991, **95**, 1579; doi:10.1002/bbpc.19910951201.
4. Gutkowski K., Anisimov M.A., Sengers J.V., J. Chem. Phys., 2001, **114**, 3133, doi:10.1063/1.1338982.
5. Schröder W., Contrib. Plasma Phys., 2012, **52**, 78; doi:10.1002/ctpp.201100104.
6. Wiegand S., Berg R.F., Levelt Sengers J.M.H., J. Chem. Phys., 1998, **109**, 4533; doi:10.1063/1.477057.
7. Wiegand S., Briggs M.E., Levelt Sengers J.M.H., Kleemeier M., Schröder W., J. Chem. Phys., 1998, **109**, 9038; doi:10.1063/1.477574.
8. Schröder W., Wagner M., Stanga O., J. Mol. Liq., 2006, **127**, 2; doi:10.1016/j.molliq.2006.03.002.
9. Hynninen A.-P., Panagiotopoulos A.Z., Mol. Phys., 2008, **106**, 2039; doi:10.1080/00268970802112160.
10. Caillol J.-M., Levesque D., Weis J.-J., J. Chem. Phys., 2002, **116**, 10794; doi:10.1063/1.1480009.
11. Luijten E., Fisher M.E., Panagiotopoulos A.Z., Phys. Rev. Lett., 2002, **88**, 185701; doi:10.1103/PhysRevLett.88.185701.
12. Kim Y.C., Fisher M.E., Panagiotopoulos A.Z., Phys. Rev. Lett., 2005, **95**, 195703; doi:10.1103/PhysRevLett.95.195703.
13. Patsahan O.V., Mryglod I.M., J. Phys.: Condens. Matter, 2004, **16**, L235; doi:10.1088/0953-8984/16/16/L01.
14. Ciach A., Phys. Rev. E, 2006, **73**, 066110; doi:10.1103/PhysRevE.73.066110.
15. Parola A., Pini D., Mol. Phys., 2011, **109**, 2989; doi:10.1080/00268976.2011.624556.
16. Schröder W., In: Ionic Soft Matter: Modern Trends and Applications, NATO ASI Series II, Henderson D., Holovko M., Trokhymchuk A. (Eds.), Springer, Dordrecht, 2004, 143–180.
17. Sengers J.V., Shanks J.G., J. Stat. Phys., 2009, **137**, 857; doi:10.1007/s10955-009-9840-z.
18. Patsahan O.V., Phys. Rev. E, 2013, **88**, 022102; doi:10.1103/PhysRevE.88.022102.
19. Patsahan O.V., Phys. Rev. E, 2014, **89**, 062143; doi:10.1103/PhysRevE.89.062143.
20. Weingärtner H., Kleemeier M., Wiegand S., Schröder W., J. Stat. Phys., 1995, **78**, 169; doi:10.1007/BF02183345.
21. Weiss V.C., Schröder W., J. Stat. Mech., 2008, P04020; doi:10.1088/1742-5468/2008/04/P04020.
22. Schröder W., Vale V.R., J. Phys.: Condens. Matter, 2009, **21**, 424119; doi:10.1088/0953-8984/21/42/424119.
23. Kristóf T., Boda D., Liszi J., Henderson D., Carlson E., Mol. Phys., 2003, **101**, 1611; doi:10.1080/0026897031000068523.
24. Ciach A., Stell G., J. Chem. Phys., 2001, **114**, 3617; doi:10.1063/1.1342814.
25. Ciach A., Stell G., Physica A, 2002, **306**, 220; doi:10.1016/S0378-4371(02)00500-9.
26. Ciach A., Stell G., Int. J. Mod. Phys. B, 2005, **19**, 3309; doi:10.1142/S0217979205032176.
27. Diehl A., Panagiotopoulos A.Z., J. Chem. Phys., 2003, **118**, 4993; doi:10.1063/1.1545095.
28. Panagiotopoulos A.Z., Kumar S.K., Phys. Rev. Lett., 1999, **83**, 2981; doi:10.1103/PhysRevLett.83.2981.
29. Zubarev D.N., Dokl. Acad. Nauk SSSR, 1954, **95**, 757 (in Russian).

30. Yukhnovsky I.R., Sov. Phys. JETP, 1958, **34**, 263 [Zh. Eksp. Teor. Fiz., 1958, **34**, 379].
31. Yukhnovskii I.R., Holovko M.F., Statistical Theory of Classical Equilibrium Systems, Naukova Dumka, Kiev, 1980 (in Russian).
32. Patsahan O., Mryglod I., Condens. Matter Phys., 2006, **9**, 659; doi:10.5488/CMP.9.4.645.
33. Patsahan O.V., Mryglod I.M., Patsahan T.M., J. Phys.: Condens. Matter, 2006, **18**, 10223; doi:10.1088/0953-8984/18/45/009.
34. Ciach A., Gózdź W.T., Stell G., Phys. Rev. E, 2007, **75**, 051505; doi:10.1103/PhysRevE.75.051505.
35. Patsahan O.V., Mryglod I.M., J. Phys. A: Math. Gen., 2006, **39**, L583; doi:10.1088/0305-4470/39/40/L02.
36. Weeks J.D., Chandler D., Andersen H.C., J. Chem. Phys., 1971, **54**, 5237; doi:10.1063/1.1674820.
37. Hansen J.P., McDonald I.R., Theory of Simple Liquids, Academic Press, London, 1986.
38. Stell G., J. Stat. Phys., 1995, **78**, 197; doi:10.1007/BF02183346.
39. Levin Y., Fisher M.E., Physica A, 1996, **225**, 164; doi:10.1016/0378-4371(95)00336-3.
40. Caillol J.-M., Mol. Phys., 2005, **103**, 1271; doi:10.1080/00268970412331332970.
41. Wagner M., Stanga O., Schröer W., Phys. Chem. Chem. Phys., 2004, **6**, 4421; doi:10.1039/B404933K.
42. Patsahan O.V., Patsahan T.M., Phys. Rev. E, 2010, **81**, 031110; doi:10.1103/PhysRevE.81.031110.
43. Goldenfeld N., Lectures on Phase Transitions and the Renormalization Group, Addison-Wesley, New-York, 1992.

Фазова поведінка газ–рідина в іонних плинах: кулонівські проти некулонівських взаємодій

О. Пацаган

Інститут фізики конденсованих систем НАН України, вул. І. Свенціцького, 1, 79011 Львів, Україна

Використовуючи теорію колективних змінних, вивчається вплив конкуренції кулонівських і дисперсних сил на фазову поведінку газ–рідина модельного іонного плину, а саме, зарядоасиметричної примітивної моделі з додатковими короткосяжними притягальними взаємодіями. Отримано в однопетлевому наближенні критичні параметри і криві співіснування в залежності від параметра α , який вимірює силу кулонівської взаємодії по відношенню до короткосяжної взаємодії. Знайдено дуже вузьку область α , обмежену з обох сторін трикритичними точками, яка відокремлює моделі з “неіонною” і “кулонівською” фазовою поведінкою. Цей результат відрізняється від наявного результату комп’ютерного моделювання, отриманого для дрібнодискретизованої ґраткової версії моделі, що розглядається.

Ключові слова: іонні плини, фазова діаграма газ–рідина, трикритична точка, кулонівські взаємодії, короткосяжне притягання